

# Lawrence Berkeley National Laboratory

## LBL Publications

### Title

Atomic resolution transmission electron microscopy of the intergranular structure of a  $Y_{2}O_{3}$ -silicon nitride ceramic

### Permalink

<https://escholarship.org/uc/item/20g3b545>

### Journal

Journal of the American Ceramic Society (ACS), 86(10)

### Author

Ritchie, R.O.

### Publication Date

2002-05-01

---

---

## **Atomic Resolution Transmission Electron Microscopy of the Intergranular Structure of a Y<sub>2</sub>O<sub>3</sub>-Silicon Nitride Ceramic**

---

---

**A. Ziegler<sup>1</sup>, C. Kisielowski<sup>2</sup>, M. J. Hoffmann<sup>3</sup>, and R. O. Ritchie<sup>1</sup>**

<sup>1</sup>Materials Sciences Division, Lawrence Berkeley National Laboratory, and  
Department of Materials Science and Engineering,  
University of California, Berkeley, CA 94720, USA

<sup>2</sup>National Center for Electron Microscopy,  
Lawrence Berkeley National Laboratory, Berkeley, CA 94720, USA

<sup>3</sup>Institut für Keramik im Maschinenbau,  
Universität Karlsruhe, D-76131 Karlsruhe, Germany

submitted to the *Journal of the American Ceramic Society*

May 2002

Work supported by the Director, Office of Science, Office of Basic Energy Sciences, Materials Sciences Division of the U.S. Department of Energy under Contract No. DE-AC03-76SF00098.

# Atomic-Resolution Transmission Electron Microscopy of the Intergranular Structure of a Y<sub>2</sub>O<sub>3</sub>-Silicon Nitride Ceramic

A. Ziegler<sup>1</sup>, C. Kisielowski<sup>2</sup>, M. J. Hoffmann<sup>3</sup>, and R. O. Ritchie<sup>1</sup>

<sup>1</sup>Materials Sciences Division, Lawrence Berkeley National Laboratory, and Department of Materials Science & Engineering, University of California, Berkeley, CA 94720, USA

<sup>2</sup>National Center for Electron Microscopy, Lawrence Berkeley National Laboratory, Berkeley, CA 94720, USA

<sup>3</sup>Institut für Keramik im Maschinenbau, Universität Karlsruhe, D-76131 Karlsruhe, Germany

**Abstract:** High-resolution transmission electron microscopy (HRTEM) employing focus-variation phase-reconstruction methods is used to image the atomic structure of grain boundaries in a silicon nitride ceramic at a resolution of 0.8 Å. Complementary energy-dispersive X-ray emission spectroscopy experiments revealed the presence of yttrium ions segregated to the 0.5 - 0.7 nm thin amorphous boundary layers that separate individual grains. Our objective here is to discern whether the yttrium ions attach to the prismatic planes of the Si<sub>3</sub>N<sub>4</sub> at the interface towards the amorphous layer, using Scherzer and phase-reconstruction imaging, as well as image simulation. Although crystal structure images from thin (<7 nm) boundary area areas, do not reveal the attachment of yttrium at these positions, lattice images from thicker areas do suggest the presence of yttrium at these sites. It is concluded that most of the yttrium atoms are located in the amorphous phase and only few atoms are attached to the prism plane of the matrix-grain/grain-boundary interface; the line concentrations of such yttrium in the latter location are estimated to be one yttrium atom every 16.8 Å.

## I. Introduction

Bulk silicon nitride (Si<sub>3</sub>N<sub>4</sub>) ceramics have been the subject of numerous investigations, in particular because their physical and mechanical properties are relevant for many potential high-temperature applications. However, the properties of silicon nitride ceramics are strongly influenced by the microstructure and the chemical composition of the grain boundaries. Indeed, the grain boundaries can be considered as the key microstructural features that control mechanical properties. For example, at low homologous temperatures, a strongly bonded grain boundary can result in high strength, but a suitably "weakened" boundary, *e.g.*, from the presence of a brittle intergranular film, invariably results in higher toughness. Similarly, at high temperatures, a grain-boundary phase with a higher melting point or high viscosity is preferable for strength retention and creep resistance.

In most silicon nitride ceramics, the ubiquitous thin grain boundaries are typically 1 to 5 nm in width, with their equilibrium size considered to be a marked function of chemical

composition [1-6]. Sintering additives and impurities, particularly rare earths<sup>1</sup>, segregate along such boundaries, and generally do not form solid solutions with either the  $\alpha$ - and  $\beta$ -phase  $\text{Si}_3\text{N}_4$  matrix. Indeed, the  $\beta$ - $\text{Si}_3\text{N}_4$  crystal structure provides a tunnel-like opening,  $\sim 0.15$  nm in diameter, along the [0001] orientation [7], which allows large additive atoms, such as  $\text{Ln}^{3+}$  ions, to diffuse through. However, a stable, detectable arrangement of such ions at these boundary locations has yet to be observed.

The chemical bonding between the prismatic surface of a silicon nitride grain and atoms of sintering additives has been modeled computationally using crystal structure data [8-10]. Using a Hartree-Fock periodic approach with extended Hückel tight-binding approximation [8,9] and molecular dynamic calculations with a pair-potential set approach [10], atomic positions and grain-boundary bonding characteristics have been determined for a variety of interface atom-coordinations. The results of these calculations indicate, for example, that Mg atoms provide electrons to fill empty energy states along the grain boundaries that derive from unsaturated interface bonds. In particular, Benco [9] states that oxygen present along grain boundaries in  $\text{Si}_3\text{N}_4$  has a destabilizing effect on the bonding characteristics and serves as a trap for sintering aids to migrate towards the grain boundaries. However, direct imaging, e.g., using high-resolution transmission electron microscopy (HRTEM), of the crystal structure at the interfacial regions, specifically to identify the positions of the additive ions, has not been achieved with truly atomic resolution. A major problem here has been that a point-to-point resolution of  $\sim 0.8$  Å is required in order to identify single atom columns in  $\text{Si}_3\text{N}_4$ , and this is at the theoretical information limit of current electron microscopes. Secondly, the imaging of grain boundaries in silicon nitride is further complicated by the formation of a thin amorphous film at the interface. Crystallization of the majority of this interfacial phase at boundary triple junctions is commonly reported, although for the more interesting thin two-grain grain-boundary films, the amorphous state has been shown to be the thermodynamically preferred condition [11].

Recent progress with HRTEM, however, has made it possible to extend the resolution of a “mid-voltage” microscope well beyond its Scherzer point-to-point resolution of 1.7 Å to an information limit of about 0.8 Å [12-15]. The procedure is based on several studies [14-27] and exploits the small information limit of a field emission TEM in a particular manner via digital image processing [28,29] to produce electron exit waves. Usually, a single HRTEM image represents a highly encoded mixture of the properties of the sample with those of the TEM. A reconstruction of the electron exit wave from a focus series of lattice images, on the other hand, allows eliminating imaging artifacts, extending resolution and simplifying image interpretation.

In this paper, we use this technique to image silicon nitride with an unprecedented resolution and a sensitivity that allows for the detection of single nitrogen columns in the  $\text{Si}_3\text{N}_4$  matrix. Specifically, we focus on the grain boundaries in a silicon nitride sintered with 2 wt.%  $\text{Y}_2\text{O}_3$  and examine the segregation of the sintering additive ions to these

---

<sup>1</sup> Exceptions here are the alpha- and beta-SiAlON additives, which are isostructural derivatives of  $\alpha$ - and  $\beta$ - $\text{Si}_3\text{N}_4$ .

interfaces. Specifically, it is found that although the yttrium ions definitely segregate to the boundaries, it was difficult to detect irrefutable evidence that the yttrium ions attach to N-terminated plane of the half-ring of the Si-hexagons that are present, we believe because the yttrium ion concentration in these locations was too low.

## II. Experimental Procedures

### (1) *Material*

The silicon nitride examined was fabricated with a newly developed two-step sintering technique, consisting of a dilatometer-controlled, gas-pressure-sintering process and a subsequent hot-isostatic pressing densification [30]. Such highly pure and controlled processing was utilized in order to permit an unambiguous investigation of the role of small quantities of sintering aids that optimize the material properties; specifically, the technique allowed for an almost impurity-free densification without the usual glass encapsulation technique.

Si<sub>3</sub>N<sub>4</sub> powder (UBE SN E10; Ube Industries, Yamaguchi, Japan) was sintered with 2 wt.% Y<sub>2</sub>O<sub>3</sub> (fine grade, HCST) to achieve a microstructure consisting of two morphologies of β-Si<sub>3</sub>N<sub>4</sub> grains, namely (i) predominantly acicular-shaped grains, with an average length of 5 μm and an aspect ratio of 8:1, and (ii) equiaxed grains, with a size of 0.5 to 1.5 μm.

Samples for examination in the TEM were prepared by grinding, dimpling, and ion milling. The low-voltage ion milling was performed with a LINDA ion mill (Technoorg LINDA, IV3H/L ion beam thinning unit, Scientific Technical Development LTD., USA) to produce foils with a thickness of <100 Å and with highly smooth surfaces (i.e., surface roughness ≤10 Å).

### (2) *Electron Microscopy*

(A) *Electron Microscope*: The HRTEM investigation was performed with a Philips CM300/FEG/UT, a 300kV microscope, equipped with a field emission electron source (FEG) and an ultra-twin objective lens of low spherical aberrations ( $C_s = 0.60$  mm) and chromatic aberrations ( $C_c = 1.3$  mm). This microscope was modified to improve its information limit, such that lattice images can be recorded aberration free to a smallest distance of about 0.8 Å [31].

The specimen stage used was a Philips double-tilt low-background holder with a tilting range of ±30°/±30°. Images were recorded digitally through an attached Gatan Image Filter (GIF) on a 2048 x 2048-pixel CCD (charge-coupled device) camera that allows for a total magnification up to 38 million times. Electron exit waves were reconstructed from series of twenty lattice images using the Philips/Brite-Euram software by Coene and Thust [28,29].

(B) *Phase Retrieval and Image Reconstruction:* An exit-wave function emanating from the back plane of the specimen can be written as a function containing an amplitude and phase relationship:

$$\psi(\mathbf{r}) = A(\mathbf{r}) \cdot \exp(-i\phi_t(\mathbf{r})), \quad (1)$$

where  $A(\mathbf{r})$  is the amplitude and  $\phi_t(\mathbf{r})$  is the phase, which depends on the specimen thickness. However, the intensity  $I$  captured on the image plane is:

$$I = \psi \cdot \psi^* = |\psi|^2, \quad (2)$$

which is why phase information is lost. The successive projection of the electron exit wave into an image plane can be written as:

$$\Phi(\mathbf{u}) = H(\mathbf{u}) \cdot \Psi(\mathbf{u}), \quad (3)$$

where  $\mathbf{u}$  is the reciprocal-lattice vector representing the spatial frequencies, and  $\Phi(\mathbf{u})$  and  $\Psi(\mathbf{u})$  are the image and specimen function respectively.  $H(\mathbf{u})$  is the contrast transfer function (CTF) that describes how contrast is transferred into the image plane. The  $H(\mathbf{u})$  function characterizes microscope parameters such as the spherical aberrations  $C_s$  of the objective lens and the defocus  $\Delta f$ . A finite spatial and temporal coherence act to damp this function and impose a limit as to which information can be transferred at 0.8 Å that lies well beyond the Scherzer point-to-point resolution:

$$\rho_s = 0.65 \cdot C_s^{1/4} \cdot \lambda^{3/4} = 0.17 \text{ nm}. \quad (4)$$

The phase retrieval procedure restores the proper amplitudes and phases of the electron exit waves down to the microscope's information limit and removes undesired effects of delocalization. In the present study, this was typically extracted from twenty lattice images recorded around an underfocus of -260 nm with a constant defocus interval of ~2.4 nm for successive lattice images.

(C) *Analytical Equipment:* Analytical investigations of the distribution of chemical elements along the grain boundary were performed on a Philips CM200/FEG transmission electron microscope. This analytical TEM is equipped with an energy dispersive X-ray emission spectrometer (EDS). Spatially resolved compositional analysis ( $Z > 5$ ) could be performed with this instrument with energy resolution of 1.36 eV for Mn  $K_\alpha$  radiation. The EDS probe diameter could be focused to a 1.2 nm small spot in order to detect the signal emanating from a 1 to 5 nm thick two-grain grain-boundary film.

### (3) *Computer Simulations*

The crystal structure and interface modeling was performed using the commercial program CrystalKit [32]. Subsequent HRTEM image simulations were performed using the structure models as input to the commercial program MacTempas [32]. Through-focus and through-thickness image simulations can be created with this program from the model crystal structures. MacTempas is based on the multislice method, whereby the structure

model is sliced perpendicular to the direction of the incident beam. The potential content of each single slice modifies the incoming electron wave, which is then projected onto the next slice and propagated through the entire structure model [33].

### III. Results and Discussion

#### (1) *Preliminary HRTEM Imaging of the Crystal Structure of Silicon Nitride*

To demonstrate the resolution and capabilities of the microscope and the phase reconstruction technique, Fig. 1 shows the experimentally reconstructed phase of the electron exit wave from the crystal structure of  $\beta$ - $\text{Si}_3\text{N}_4$ , projected along the [0001] direction [13]. Experimentally, sample tilt is a most limiting factor to obtain such a high-resolution image. All details of the modeled structure of  $\beta$ - $\text{Si}_3\text{N}_4$ , shown in schematic form in Fig. 2a, can be identified in the phase-reconstructed image; indeed, the hexagonal crystal structure can be directly superimposed on the experimental image of Fig. 1. Simulation of the electron exit wave, using the model structure of  $\text{Si}_3\text{N}_4$ , confirms this assignment (inset in Fig. 1). The silicon columns appear as brighter spots because silicon has a larger scattering power than nitrogen. Two nitrogen positions are visible in this projection. The first one is clearly separated among three silicon columns and the second one appears as a shoulder on the silicon columns. A line scan taken across phase maxima of a close Si-N pair in the phase reconstructed image (Fig. 2b) reveals the presence of nitrogen and demonstrates the resolution of this imaging technique. However, the nitrogen signal is weak at this thickness and is not fully separated from the silicon signal.

#### (2) *HRTEM Imaging of the Crystal Structure of the Grain Boundaries*

(A) *Phase Reconstruction Imaging:* To study the atomic structure of the grain boundaries in  $\text{Si}_3\text{N}_4$ , thin two-grain boundaries were examined utilizing the exit wave reconstruction process. This technique proved to be successful for imaging the intergranular phase and results are described below in terms of a current theoretical model [10] for the interfacial structure of silicon nitride.

The initial results of reconstructed phase images of such thin boundaries are presented in Figs. 3a and 4a; compared to the corresponding Scherzer defocus images, shown in Figs. 3b and 4b, a significant gain in information is apparent. In both examples, a residual tilt of 0.87 and 1.05 mrad can be detected in the phase-reconstructed images in Figs. 3a and 4a, respectively. This affects the intensity distribution in the lattice images and the reconstructed electron exit wave. A comparison of the Scherzer defocus image with computer-simulated images allows for an estimation of experimental parameters, specifically in these examples, defocus,  $\Delta f$ , and sample thickness,  $t$ , in the sampling area. In Fig. 3,  $\Delta f = -50$  nm and  $t \sim 10$ -20 Å, whereas for Fig. 4,  $\Delta f = -70$  nm and  $t \sim 70$ -80 Å. In interpreting these images, it can be deduced that the grain boundary is amorphous and  $\sim 5$ -7 Å in thickness. Of note in Fig. 3a is the shape of the Si-hexagons in the  $\beta$ - $\text{Si}_3\text{N}_4$  grain to the right that reach into the amorphous intergranular layer. The reconstructed image reveals rather incomplete, not fully closed, Si-hexagons extending into the amorphous

grain boundary. This observation suggests the possibility of dangling bonds connecting the  $\beta$ - $\text{Si}_3\text{N}_4$  grain to segregated ions in the amorphous grain boundary, although no segregated sintering additive ions can be seen in these reconstructed images at any particular atom position along the interface. Consequently, salient criteria and imaging conditions must be met in order to identify atom segregation along the interface, as addressed below in light of theoretical assumptions and calculations regarding the near-matrix grain structure [10,34-36].

According to the first-principles molecular orbital (MO) calculations performed by Nakayasu *et al.* [10], rare-earth ions show a tendency to attach to the prismatic plane of  $\beta$ - $\text{Si}_3\text{N}_4$  grains. The calculations assume a nitrogen-terminated prism plane, as illustrated schematically in Fig. 5. Their results indicate that the chemical bond strength, evaluated by the overlap population, is increased by the presence of any rare-earth ion at the prismatic interface, covering a range of ionic radii, from 0.85Å (Yb) to 1.06Å (La). The high-purity silicon nitride studied in the present investigation contains yttrium as a sintering additive with an ionic radius of 0.89Å, similar to the rare-earth ion holmium. It is therefore anticipated that yttrium should show similar behavior to other rare-earth ions and attach preferably to the prismatic planes of  $\text{Si}_3\text{N}_4$ .

Accordingly, attempts were made to image this near-matrix-grain structure in the amorphous layer to identify any epitaxial-like attachment of impurity or sintering-aid ions to the prismatic  $\beta$ - $\text{Si}_3\text{N}_4$  planes. Since yttrium is a heavier atom than silicon and nitrogen, this should yield stronger electron scattering and image contrast, *e.g.*, brighter spots, and would enable detection of individual yttrium atoms along the grain boundary. However, neither the Scherzer nor the phase-reconstructed images in Figs. 3 and 4 exhibit such brighter spots at the preferred locations along the prismatic planes. Thus, the question arises if there are certain imaging conditions under which these ions will show up in a phase-reconstructed image. Salient criteria that have to be met for such Scherzer and phase-reconstructed HRTEM imaging include the presence and concentration of the ion in the boundary, the ion-column density, specimen thickness and electron oscillation wavelength in the specimen [37]. The latter three are addressed below in section III.2.B on computer simulation.

With respect to the concentration, as the  $\text{Si}_3\text{N}_4$  investigated here contains only a small amount (2 wt%) of  $\text{Y}_2\text{O}_3$ , it was necessary to confirm that sufficient yttrium ions were present along boundaries; this was achieved using an EDS line scan taken across thin two-grain grain boundaries. The results, shown in Fig. 6, clearly demonstrate that yttrium is segregated to the interface. However, not all of the ions detected via EDS are attached in columns to the prism planes. In fact, it is expected that most of the yttrium atoms are located in the amorphous phase and only few atoms are attached to the prism plane of the matrix grain-grain boundary interface. For imaging, it is the density of these ions, attached to the prism plane in a column parallel to the direction of the incident electron beam that is important. A denser column of ions causes stronger scattering of the incident electrons. For phase-reconstructed imaging, a conflict can arise when the column density is low. Specifically, if the bonding characteristics are such that there is a large separation between yttrium ions attached to the prism plane along the columns, this requires using a thicker



sample to exceed a minimum ion density for good imaging contrast. However, foils much thicker than 100Å are not optimal for phase reconstruction purposes because of loss of resolution.

Nevertheless, the Scherzer and phase-reconstructed images of a grain boundary in a sample area, slightly thicker than the recommended upper limit of 100Å, are presented in Figs. 7a and b, respectively. The Scherzer defocus image displays bright spots that are arranged in a periodic manner close to the prismatic plane. It is difficult to determine the precise specimen thickness on this image because of the relatively large tilt. The resulting phase reconstructed image reveals that the bright spots have disappeared, and the half-rings of the Si-hexagons are no longer visible. Interestingly though, the bright spots in Fig. 7a exhibit a very regular periodicity, and hence the question arises whether those spots are a result of yttrium atoms attached to the prismatic plane or due to the large delocalization of information in a field emission microscope.

(B) *Computer Simulations:* To better understand the observed phenomenon, computer simulations were performed of this particular grain boundary (with the same grain orientations and specimen tilt), with the objective of matching the simulations to the experimental results. Based on Nakayasu *et al.*'s calculations [10], the simulation was performed with a grain boundary where the yttrium ions were positioned at nitrogen terminated  $\beta$ -Si<sub>3</sub>N<sub>4</sub> prism planes (Fig. 8). The remainder of the grain boundary was modeled as a region,  $\sim 5\text{\AA}$  in width, filled with randomly oriented silicon and oxygen atoms imitating a SiO<sub>2</sub>-rich amorphous phase. The resulting simulated Scherzer defocus image and the corresponding simulated phase reconstruction are presented, respectively, in Figs. 9a and b. The calculation, employing an yttrium ion separation of 2.8Å and a specimen thickness of 130Å yields very similar images to the experimental ones in Figs. 7a and b. However, it is important to note that only a yttrium atom separation of 2.8Å yielded helpful results; larger atom separations did not prove to be useful. The simulated Scherzer defocus image (Fig. 9a) shows very similar bright spots at almost the same locations and with the same periodicity as in the experimental Scherzer image (Fig. 7a). In contrast, the simulated exit wave image (Fig. 9b) does not exhibit bright spots, as in the experimental image in Fig. 7b, since delocalization effects are removed. It does show, however, that the open Si-hexagon rings are present and reach into the amorphous grain boundary, although the rings are hidden underneath amorphous-like looking features in the image. Varying the sample tilt in the simulation did not make the half-rings reappear in the reconstructed image. Figs. 10a and b show a direct comparison of these experimental and simulated images. The fact that the lower parts, *i.e.*, the Si<sub>3</sub>N<sub>4</sub> crystal opposite the grain boundary, in both the experimental Scherzer and the phase-reconstructed images look different from the simulations is of concern and is currently being investigated. One reason is that with simulated images, one has always a much better detail visibility than with the corresponding experimental images.

At this stage, one must conclude that the experimental images, in particular the phase reconstruction image in Fig. 7b, do not provide irrefutable evidence that yttrium is attached to the prismatic planes. Indeed, since the bright spots seen in the Scherzer defocus image disappear after reconstruction, it is certainly feasible that they are associated with artifacts

of the field emission gun and the contrast transfer function. Yttrium would be expected to show up in the reconstruction if it is located at the indicated site, since it is almost three times heavier than silicon. This would be most apparent in thin samples where the signal-to-noise ratio is best; however, thin sample areas are shown in Figs. 3 and 4 and no yttrium ions can be identified. *However, an alternative explanation for the apparent absence of Y in these locations is that its line density is too low.* This is especially pertinent considering the presence of the amorphous grain-boundary layer, which can lead to increased noise levels and lower sensitivity limits.

To determine the ion-column density that is required for yttrium atoms to show up in a phase-reconstructed image, computer simulations of phase reconstructed exit wave images were performed. Yttrium atoms were positioned according to Nakayasu *et al.*'s calculations [10] at the N-terminated prism plane of a  $\text{Si}_3\text{N}_4$  crystal. The yttrium ion-column density was varied by changing the relative separation between Y atoms, from one yttrium atom every  $2.8\text{\AA}$  to one yttrium atom every  $16.8\text{\AA}$ . The sample thickness was then varied for each ion-column density from  $10$  to  $100\text{\AA}$ . This allowed for an examination of the present Bloch wave oscillations on the phase reconstructed image.

The oscillation is caused by the interaction of the incoming electron waves with material in zone axis orientation and is strongly dynamic. The propagating electron wave exhibits a specific distance – an extinction distance  $\zeta$  - that depends on the scattering power of a specific column of atoms. Lighter atoms produce a longer extinction distance compared to heavier atoms. Moreover, the extinction distance scales with  $Z/d^2$ , where  $Z$  is the atomic number and  $d$  is atom separation [37]. Maximum image contrast and thus visibility at the exit plane occur when the specimen thickness coincides with one half of an extinction oscillation. The approximated half extinction distance for a column of Si atoms with a density of one Si atom/ $2.8\text{\AA}$  is  $\zeta \sim 75\text{\AA}$  [38]. In comparison, the extinction distance is approximated to  $\zeta \sim 26\text{\AA}$  for yttrium at a separation of  $2.8\text{\AA}$ , *i.e.*, for one yttrium atom per  $\text{Si}_3\text{N}_4$  unit cell,

Fig. 11a shows a few simulated exit wave images for a line density of one Y-atom every  $2.8\text{\AA}$ . The oscillation of the Y signal with sample thickness can be clearly seen. The graph in Fig. 12a shows how the extinction distance for yttrium varies with column density in relation to Si. Assuming a sample thickness of  $\sim 75\text{\AA}$  (Fig. 4), a vertical line can be drawn at  $75\text{\AA}$ . Marking the intersection with the Si curve this represents the maximum signal visibility for Si for this particular sample thickness,  $0.9\text{rad}$  (Fig. 12b). On the other hand, any atom signal will become invisible when it is comparable to the noise level,  $0.1\text{rad}$ , represented here by the amorphous intergranular phase (Fig. 12b) and the lower horizontal line drawn in Fig. 12a. Therefore, a lower visibility limit can be established. Accordingly, for a  $75\text{\AA}$  thick sample, yttrium will become invisible when its column density is less than one Y-atom every  $14.0\text{\AA}$ . For thinner sample areas, the Y-visibility limit is raised to higher Y-atom column densities. For example, the reconstructed exit wave image in Fig. 3 (sample thickness  $10$ - $20\text{\AA}$ ) would require a Y-atom column density of more than one Y-atom per  $7.0\text{\AA}$  in order to exhibit any Y signal. Thus, it can be concluded that for the imaging of low levels of yttrium concentrations at grain boundaries, thicker specimens are required. However, in thick crystal regions, reliable phase

reconstructions are much more difficult to achieve, for reasons that are currently being investigated.

However, some evidence for the presence of Y can be produced in the traditional manner, namely by recording lattice images at Scherzer defocus, as for example in Fig. 7a, that are then compared with image simulations. It is important to note though that Scherzer lattice images in a field emission microscope can often be misleading due to the large beam coherence and the complicated contrast transfer function. By default, less information is seen in a single lattice image than in a reconstructed image because the CTF removes information and creates delocalization. Commonly, these effects can light up edges such that the bright spots along the boundaries could be associated with imaging artifacts.

Scherzer image simulations, though, do show that such bright and periodic spots do appear in thicker ( $\sim 130\text{\AA}$ ) specimens along the grain boundaries when yttrium is placed at the N-terminated prism planes of a  $\text{Si}_3\text{N}_4$  crystal. This is the result of an analysis of two different grain-boundary configurations: (i) a grain boundary with Y ions positioned at the N-terminated prism planes, and (ii) a grain boundary without Y ions.

From Fig. 13, it is apparent that the image of the Y-containing grain boundary displays an array of double bright spots along the interface at a specimen thickness of  $130\text{\AA}$ , resembling the experimental Scherzer defocus images in Fig. 9a. The location of the individual atoms can be seen on the atom position overlay; they are not located directly at the interface but one half Si-hexagon ring away from it. The same grain boundary without Y instead shows no bright spots. These simulations suggest that the bright spots might represent yttrium ions at specific atomic positions along the grain boundary. However, very careful interpretation of the Scherzer images is required because the true location of the yttrium ions may not be identical to the location of the bright spots. The appearance of the spots is a result of the combination of electrons scattering off the yttrium ions and the effects of the path of information transfer through the TEM, *i.e.*, from lens aberrations, on the electrons.

The results of the computer simulation show that, in theory, yttrium is detectable in the reconstructed image even though the signal is small. Moreover, it is known from the EDS results in Fig. 6 that yttrium is definitely present in the grain boundaries. However, the HRTEM imaging results are less conclusive. In particular, the interpretation of Scherzer images is difficult. The main problem with the interpretation of such lattice images is that there are no unique solutions. Even if it could be shown that the presence of Y atoms at the prismatic interface causes fringes and bright spots at the grain-boundary edges, it does not exclude the possibility that, for example, yttrium in the amorphous layer could also cause such fringes and spots. Hence, no direct HRTEM evidence can be presented at this stage to prove that specifically yttrium attaches preferentially along the prismatic interface in detectable concentrations. However, as it appears that most of the yttrium is in the amorphous phase, we believe that this lack of direct evidence is because only a few atoms, *i.e.*, one yttrium atom every  $16.8\text{\AA}$ , are attached in this location.

Determination of the position of yttrium atoms in the amorphous layer is complex, and the corresponding image simulations were not attempted in this work. Nevertheless, it is important to note that yttrium atoms, positioned at certain sites along the interface in a narrow range of sample thicknesses, do cause specific features to appear in the Scherzer defocus image that do not show up in simulated images of an yttrium-free grain boundary.

#### IV. Conclusions

Focus-variation image-reconstruction high-resolution transmission electron microscopy (HRTEM) has been used to image the atomic structure of a silicon nitride ceramic to a resolution of  $0.8\text{\AA}$ , *i.e.*, at the theoretical information limit of the microscope. Using both complementary Scherzer and phase-reconstructed images, these techniques have been specifically applied to investigate the structure of the grain boundaries in a high-purity, dilatometer-controlled gas-pressure-sintered  $\text{Si}_3\text{N}_4$  containing 2 wt%  $\text{Y}_2\text{O}_3$  as a sintering additive.

Based on complementary EDS studies, it was confirmed that the yttrium ions had segregated to, and were present in, the grain boundaries. From theoretical studies in the literature [10], the precise location of these ions has been assumed to be at the N-terminated plane of the half-ring of the Si-hexagon, *i.e.*, on the prism plane of the matrix grain-grain boundary interface; in addition, most of the yttrium atoms were expected to be located in the thin amorphous film along the boundary.

Images of a thin two-grain boundary resulted in a clear view of half-rings reaching into the amorphous grain boundary suggesting that yttrium could indeed attach to those locations. However, direct proof via HRTEM imaging for could not be obtained. We argue that in thin ( $<75\text{\AA}$ ) crystals, the estimated yttrium line density of one Y atom every  $16.8\text{\AA}$  is too low to produce a signal above the correlated noise from the amorphous part of the interface. Only indirect confirmation that yttrium ions were positioned at the half-plane of the Si-hexagon was possible from computer simulations of Scherzer HRTEM images recorded at larger foil thicknesses. However, we conclude that most of the yttrium atoms are located in the amorphous boundary phase with only few atoms, specifically one yttrium atom every  $16.8\text{\AA}$ , attached to the prism plane of the matrix-grain/grain-boundary interface.

**Acknowledgments:** This work was supported by the Director, Office of Science, Office of Basic Energy Sciences, Division of Materials Sciences and Engineering, of the U.S. Department of Energy under Contract No. DE-AC03-76SF00098. The authors wish to thank Dr. Mike O’Keefe for developing the sub-Ångström resolution microscopy facilities at the National Center for Electron Microscopy (NCEM), Chris Nelson, of NCEM, for help with some of the early HRTEM work, and Dr. Rowland Cannon for helpful discussions.

## References

- [1] Clarke, D. R., "On the Equilibrium Thickness of Intergranular Glass Phases in Ceramic Materials," *J. Am. Ceram. Soc.*, **70** [1], 15-22 (1987).
- [2] Wang, C. M., Pan, X., Hoffmann, M. J., Cannon, R. M. and Rühle, M., "Grain Boundary Films in Rare-Earth-Glass-Based Silicon Nitride," *J. Am. Ceram. Soc.*, **79** [3], 788-92 (1996).
- [3] Gu, H., Pan, X., Cannon, R. M. and Rühle, M., "Dopant Distribution in Grain-Boundary Films in Calcia-Doped Silicon Nitride Ceramics," *J. Am. Ceram. Soc.*, **81** [12], 3125-35 (1998).
- [4] Clarke, D. R., Shaw, T. M., Philipse, A. P. and Horn R. G., "Possible Electrical Double-Layer Contribution to the Equilibrium Thickness of Intergranular Glass Films in Polycrystalline Ceramics," *J. Am. Ceram. Soc.*, **76** [5], 1201-04 (1993).
- [5] Kleebe, H.J., Cinibulk, M.K., Cannon, R.M. and Rühle, M., "Statistical Analysis of the Intergranular Film Thickness in Silicon Nitride Ceramics," *J. Am. Ceram. Soc.*, **76** [8], 1969-77 (1993).
- [6] Kleebe, H. J., Cinibulk, M. K., Tanaka, I., Bruley, J., Cannon, R. M., Clarke, D. R., Hoffmann, M. J. and Rühle, M., "High-Resolution Electron Microscopy Observation of Grain-Boundary Films in Silicon Nitride Ceramics," *Mat. Res. Soc. Symp. Proc.*, vol. 287, Material Research Society, pp. 65-78 (1993).
- [7] Wang, C. M., Pan, X., Gu, H., Duscher, G., Hoffmann, M. J., Cannon, R. M. and Rühle, M., "Transient Growth Bands in Silicon Nitride Cooled in Rare-Earth-Based Glass," *J. Am. Ceram. Soc.*, **80** [6], 1397-404 (1997).
- [8] Dudsek, P. and Benco, L', "Cation-Aided Joining of Surfaces of  $\beta$ -Silicon Nitride: Structural and Electronic Aspects," *J. Am. Ceram. Soc.*, **81** [5], 1248-54 (1998).
- [9] Benco, L', "Chemical bonding at grain boundaries: MgO on  $\beta$ -Si<sub>3</sub>N<sub>4</sub>," *Surface Science*, **327**, 274-84 (1995).
- [10] Nakayasu, T., Yamada, T., Tanaka, I., Adachi, H. and Goto S., "Calculation of Grain-Boundary Bonding in Rare-Earth-Doped  $\beta$ -Si<sub>3</sub>N<sub>4</sub>," *J. Am. Ceram. Soc.*, **81** [3], 565-70 (1998).
- [11] Ackler, H. D. and Chiang, Y. M., "Model Experiment on Thermodynamic Stability of Retained Intergranular Amorphous Films," *J. Am. Ceram. Soc.*, **80** [7], 1893-96 (1997).
- [12] Kisielowski, C., Nelson, E. C., Song, C., Kilaas, R., and Thust, A., "Aberration Corrected Lattice Imaging with Sub-Ångström Resolution," *Microscopy and Microanalysis*, **6**, 16 (2000).
- [13] Ziegler, A., Kisielowski, C. and Ritchie, R.O., "Imaging of the Crystal Structure of Silicon Nitride at 0.8 Ångström Resolution," *Acta Mat.* **50** [3] 565-574 (2002).
- [14] O'Keefe, M. A., Hetherington, C. J. D., Wang, Y. C., Nelson, E. C., Turner, J. H., Kisielowski, C., Malm, J. O., Mueller, R., Ringnalda, J., Pam, M. and Thust, A., "Sub Ångström High-Resolution Transmission Electron Microscopy at 300 kV," *Ultramicroscopy* **89** [4] 215-241 (2001).
- [15] Kisielowski, C., Hetherington, C. J. D., Wang, Y. C., Kilaas, R., O'Keefe, M. A. and Thust, A., "Imaging Columns of the Light Elements C, N, and O with Sub-Ångström Resolution," *Ultramicroscopy* **89** [4] 243-263 (2001).

- [16] Lichte, H., "Electron Holography I. Can Electron Holography Reach 0.1 nm Resolution?," *Ultramicroscopy*, **47** [1-3] 223-30 (1992).
- [17] Van Dyck, D., Op de Beeck, M. and Coene, W. M. J., "A new approach to object wavefunction reconstruction in electron microscopy," *Optik*, **93**, 103-09 (1993).
- [18] Coene, W. M. J., Janssen, G., Op de Beeck, M. and Van Dyck, D., "Phase Retrieval through Focus Variation for Ultra-Resolution in Field-Emission Transmission Electron Microscopy," *Phys. Rev. Lett.*, **69** [26] 3743-46 (1992).
- [19] Op de Beeck, M., Van Dyck, D. and Coene, W. M. J., "Wave Function Reconstruction in HRTEM; The Parabola Method," *Ultramicroscopy*, **64**, 167-83 (1996).
- [20] Kirkland, E. J., "Improved High-Resolution Image Processing of Bright Field Electron Micrographs I. Theory," *Ultramicroscopy*, **15** [3] 151-72 (1984).
- [21] Kirkland, E. J., Scanning Microscopy Suppl. II (1988), Proc. 6<sup>th</sup> Pfefferkorn Conf. on Image and Signal Processing in Electron Microscopy, Niagara Falls, Canada, pp. 139 (1987).
- [22] Saxton, W. O., "Correction of artifacts in linear and nonlinear high resolution electron micrographs," *J. Microsc. Spectrosc. Electron.*, **5**, 665 (1980).
- [23] Van Dyck, D., Lichte, H. and van der Mast, K. D., "Sub-Ångström Structure Characterization: the Brite-Euram Route Towards One Ångström," *Ultramicroscopy*, **64**, 1-15 (1996).
- [24] Op de Beeck, M. and Van Dyck, D., "Direct Structure Reconstruction in HRTEM," *Ultramicroscopy*, **64**, 153-65 (1996).
- [25] Buist, A. H., van den Bos, A. and Miedema, M. A. O., Optimal Experimental Design for Exit Wave Reconstruction from Focal Series in TEM," *Ultramicroscopy*, **64**, 137-52 (1996).
- [26] Tang, D., Zandbergen, H. W., Jansen, J., Op de Beeck, M. and Van Dyck, D., "Fine-Tuning of the Focal Residue in Exit-Wave Reconstruction," *Ultramicroscopy*, **64**, 265-76 (1996).
- [27] Thust, A. Overwijk, M. H. F., Coene, W. M. J. and Lentzen, M., "Numerical Correction of Lens Aberrations in Phase-Retrieval HRTEM," *Ultramicroscopy*, **64**, 249-64 (1996).
- [28] Coene, W. M. J., Thust, A. Op de Beeck, M. and Van Dyck, D., "Maximum-Likelihood Method for Focus-Variation Image Reconstruction in High Resolution Transmission Electron Microscopy," *Ultramicroscopy*, **64**, 109-35 (1996).
- [29] Thust, A., Coene, W. M. J., Op de Beeck, M. and Van Dyck, D., "Focal-Series Reconstruction in HRTEM: Simulation Studies on Non-Periodic Objects," *Ultramicroscopy*, **64**, 211-30 (1996).
- [30] Hoffmann, M. J., Geyer, A., Oberacker, R., "Potential of the Sinter-HIP-Technique for the Development of High-Temperature Resistant Si<sub>3</sub>N<sub>4</sub>-Ceramics", *J. Euro. Ceram. Soc.*, **19**, 2359-66 (1999).
- [31] Wang, Y. C., Fitzgerald, A., Nelson, E. C., Song, C., O'Keefe, M. A., and Kisielowski, C., "Correction of the Three-Fold Astigmatism and Lattice Imaging with Information Below 100 pm," *Microscopy and Microanalysis*, **5**, 822 (1999).
- [32] The CrystalKit and MacTempas packages are both available from Total Resolution, National Center for Electron Microscopy, Lawrence Berkeley National Laboratory, Berkeley (California).

- [33] O'Keefe, M. A., Kilaas, R. "Advances in high-resolution image simulation," Scanning Microscopy, suppl. (no. 2), in: Image and Signal Processing in Electron Microscopy, 6th Pfefferkorn Conference, Niagara Falls, Ont., Canada, 28 April-2 May 1987, p.225 (1988).
- [34] Kaneko, K., Yoshia, M., Tanaka, I. and Tsurekawa, S., "Chemical Bonding of Oxygen in Intergranular Amorphous Layers in High-Purity  $\beta$ -SiC Ceramics," *Acta Mater.*, **47** [4] 1282-87 (1999).
- [35] Yoshiya, M., Tanaka, I. and Adachi, H., "Energetical Role of Modeled Intergranular Glassy Film in  $\text{Si}_3\text{N}_4$ - $\text{SiO}_2$  Ceramics," *Acta Mater.*, **48**, 4641-45 (2000).
- [36] Yoshiya, M., Adachi, H. and Tanaka, I., "Interpretation of Si- $L_{2,3}$  Edge Electron Energy Loss Near Edge Structures (ELNES) from Intergranular Glass Film of  $\text{Si}_3\text{N}_4$  Ceramics," *J. Am. Ceram. Soc.*, **82** [11], 3231-36 (1999).
- [37] Van Dyck, D. and Chen, J. H., "A Simple Theory for Dynamical Electron Diffraction in Crystals," *Sol. State Comm.*, **109**, 501-05 (1999).
- [38] Kisielowski, C., Jinschek, J., Mitsuishi, K., Dahmen, U., Lentzen, M., Ringnald, J. and Fliervoet, T., "Exit wave reconstruction, Cs correction and Z-contrast microscopy: Comparative strengths and limitations," *submitted to 15<sup>th</sup> ICEM*, 2002.

## LIST OF FIGURE CAPTIONS

Figure 1: The phase-reconstructed image shows the crystal structure of silicon nitride projected along [0001]. The individual atom positions of Si and N in the hexagonal structure can be discerned and matched directly to the crystal structure model that was used to simulate the electron exit wave, see inset.

Figure 2: The hexagonal crystal structure shown displays the smallest projected distance between a Si and a N atom,  $0.8\text{\AA}$  (a). This small distance can be resolved with the focus variation image reconstruction technique as a profile line taken across a close Si-N pair in the phase reconstructed image reveals the two atom positions (b). The Fourier components of the transformed lattice image extend into the sub-Ångström region (c) [13].

Figure 3: The phase-reconstructed (a) and the corresponding Scherzer defocus image (b) of a grain boundary are shown. The thickness in this sample area can be determined to  $10\text{-}20\text{\AA}$ . Note the shape of the Si-hexagons in the phase-reconstructed image; they are not fully closed and extend into the amorphous phase. The thickness of the amorphous grain boundary layer can be approximated  $5\text{-}7\text{\AA}$ .

Figure 4: The phase-reconstructed (a) and the corresponding Scherzer defocus image (b) of a second grain boundary in a thicker sample area are shown. Sample thickness is determined to  $70\text{-}80\text{\AA}$ .

Figure 5: The model crystal structure shows the N-terminated prism plane facing the amorphous grain boundary phase. Segregated ions of sintering additives, here yttrium, do attach to these planes according to the simulations of Nakayasu *et al.* [10].

Figure 6: EDS line-scan taken across a thin grain boundary reveals the presence of yttrium ions segregated to the amorphous interface layer. It is expected that most of these Y-ions are not attached to the prism plane, instead they are located in the thin amorphous grain boundary layer.

Figure 7: The Scherzer defocus (a) and the corresponding phase-reconstructed image (b) of a grain boundary are shown. The sample in this area is estimated to be thicker than the recommended specimen thickness for optimum phase reconstruction results. The Scherzer image displays bright spots that exhibit a very regular periodicity. These features disappear though in the phase reconstructed image.



Figure 8: Grain boundary model used for computer simulation of the Scherzer and phase reconstruction images of Fig 7. Both crystals adjacent to the amorphous grain boundary layer are oriented exactly as in the experimental images.

Figure 9: The simulated Scherzer defocus (a) and the corresponding simulated phase-reconstructed image (b) of the grain boundary from Fig. 7 are shown.

Figure 10: A direct comparison of the experimental and the computer-simulated images is presented. The images match well and similar features can be discerned.

Figure 11: An array of computer-simulated images shows how the Y-signal oscillates when the sample thickness is varied. The brightness of the spot created by the Y-atom changes with thickness; it oscillates with the extinction distance  $\zeta$ .

Figure 12: The graph shows how the extinction distance varies with line density and how Y compares to Si (a). For visibility criteria the noise level, (0.1rad) represented here by the amorphous phase and the maximum visible signal, (0.9rad) represented here by Si, are determined (b). A line density that results in a smaller signal than the noise level cannot be identified anymore in a TEM image.

Figure 13: Simulated Scherzer defocus images of a grain boundary with and without yttrium at certain atomic positions (atom overlay) display different features. The array of bright spots in the image of the yttrium-containing grain boundary resembles the experimentally obtained Scherzer defocus image.

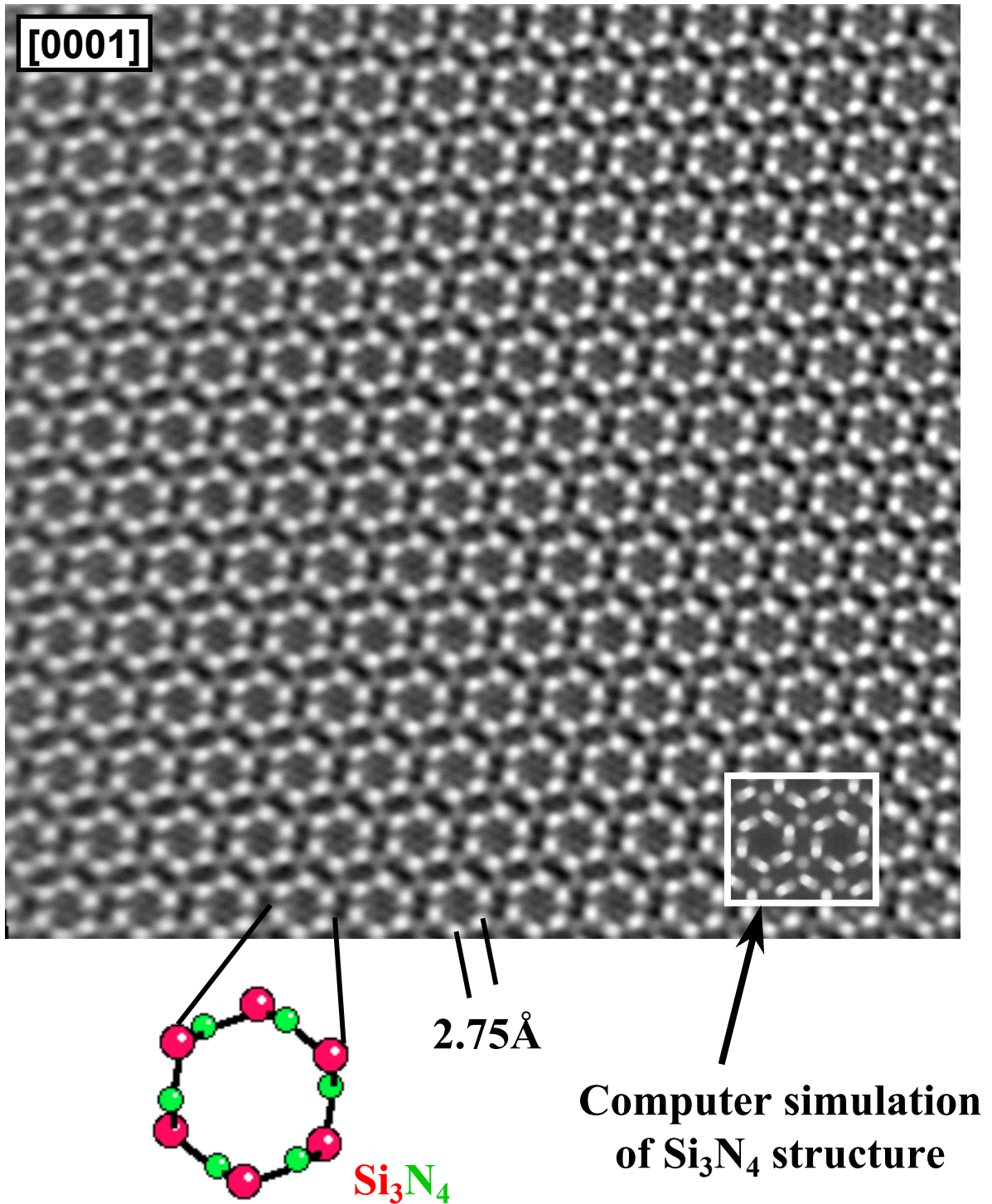
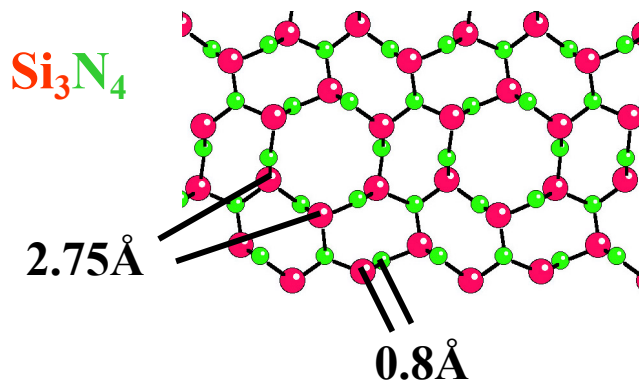


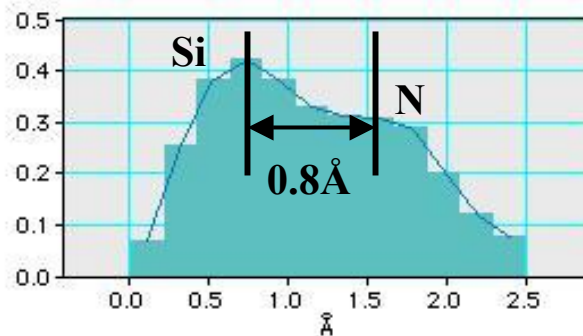
Figure 1

The phase-reconstructed image shows the crystal structure of silicon nitride projected along  $[0001]$ . The individual atom positions of Si and N in the hexagonal structure can be discerned and matched directly to the crystal structure model that was used to simulate the electron exit wave, see insert.

(a) **Si<sub>3</sub>N<sub>4</sub> crystal structure**



(b) **Profile across Si-N**



(c) **[0001]**

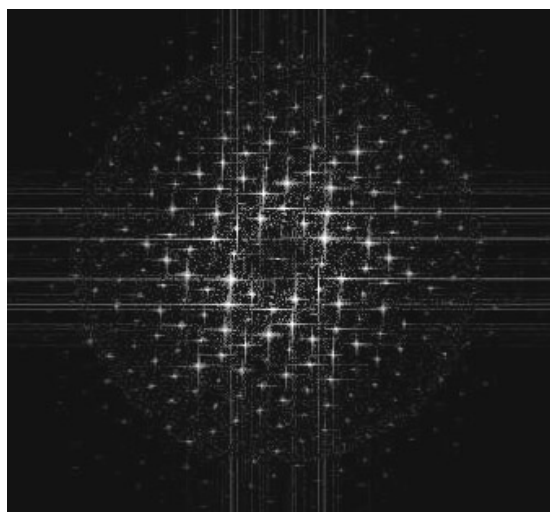


Figure 2

The hexagonal crystal structure shown displays the smallest projected distance between a Si and a N atom, 0.8 Å (a). This small distance can be resolved with the focus variation image reconstruction technique as a profile line taken across a close Si-N pair in the phase reconstructed image reveals the two atom positions (b). The Fourier components of the transformed lattice image extend into the sub-Ångström region (c).

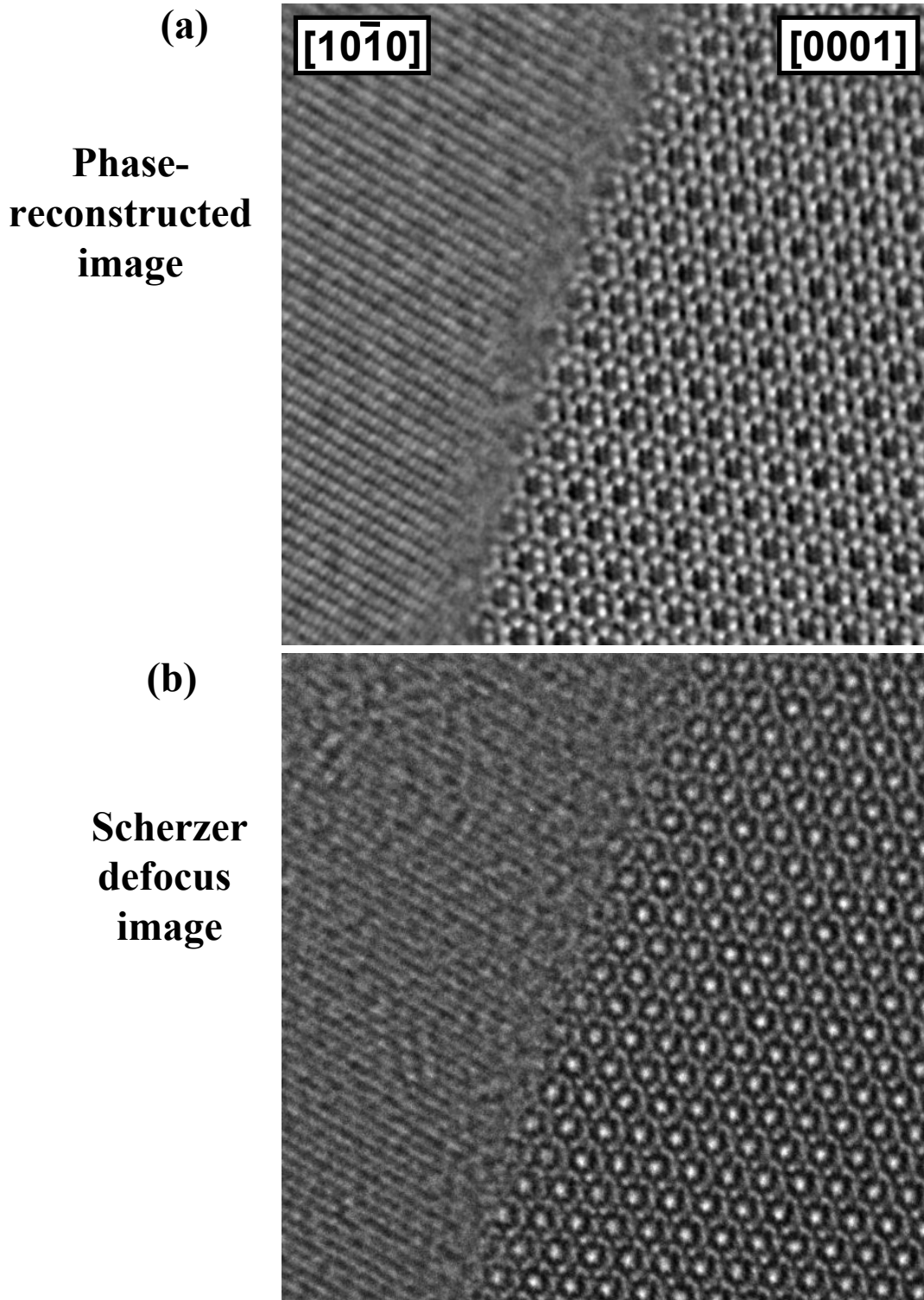


Figure 3  
The phase-reconstructed (a) and the corresponding Scherzer defocus image (b) of a grain boundary are shown. The thickness in this sample area can be determined to 10-20Å. Note the shape of the Si-hexagons in the phase-reconstructed image; they are not fully closed and extend into the amorphous phase. The thickness of the amorphous grain boundary layer can be approximated 5-7Å.

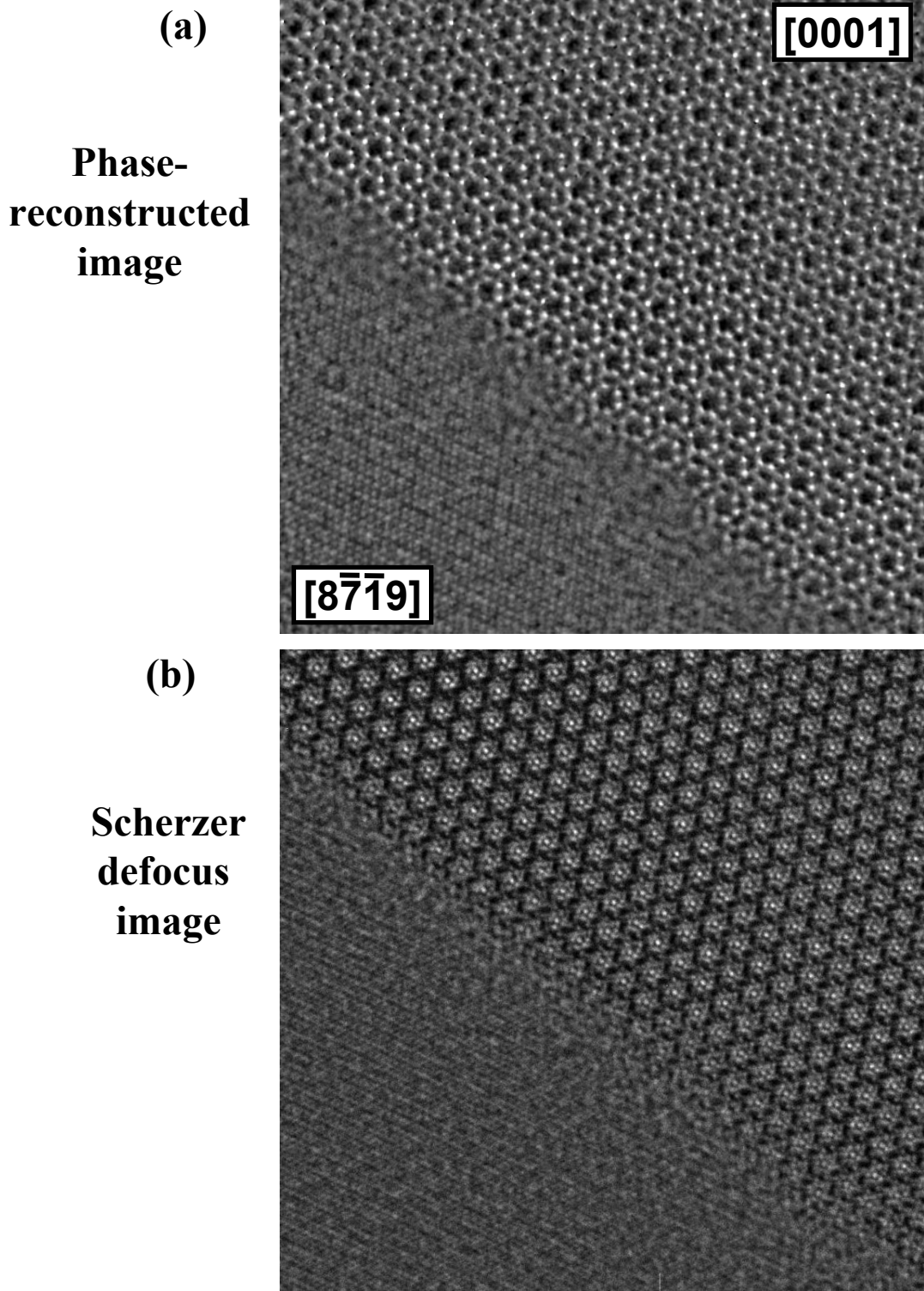


Figure 4  
The phase-reconstructed (a) and the corresponding Scherzer defocus image (b) of a second grain boundary in a thicker sample area are shown. Sample thickness is determined to 70-80Å.

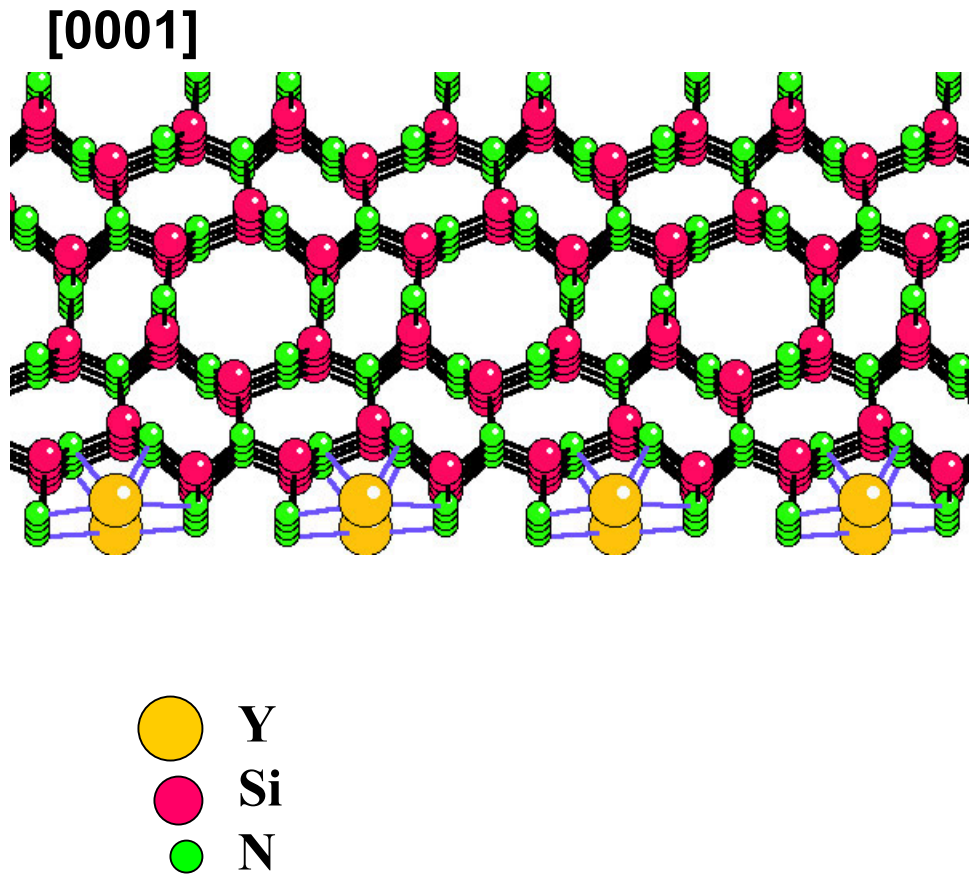


Figure 5

The model crystal structure shows the N-terminated prism plane facing the amorphous grain boundary phase. Segregated ions of sintering additives, here yttrium, do attach to these planes according to Nakayasu *et al.* [10].

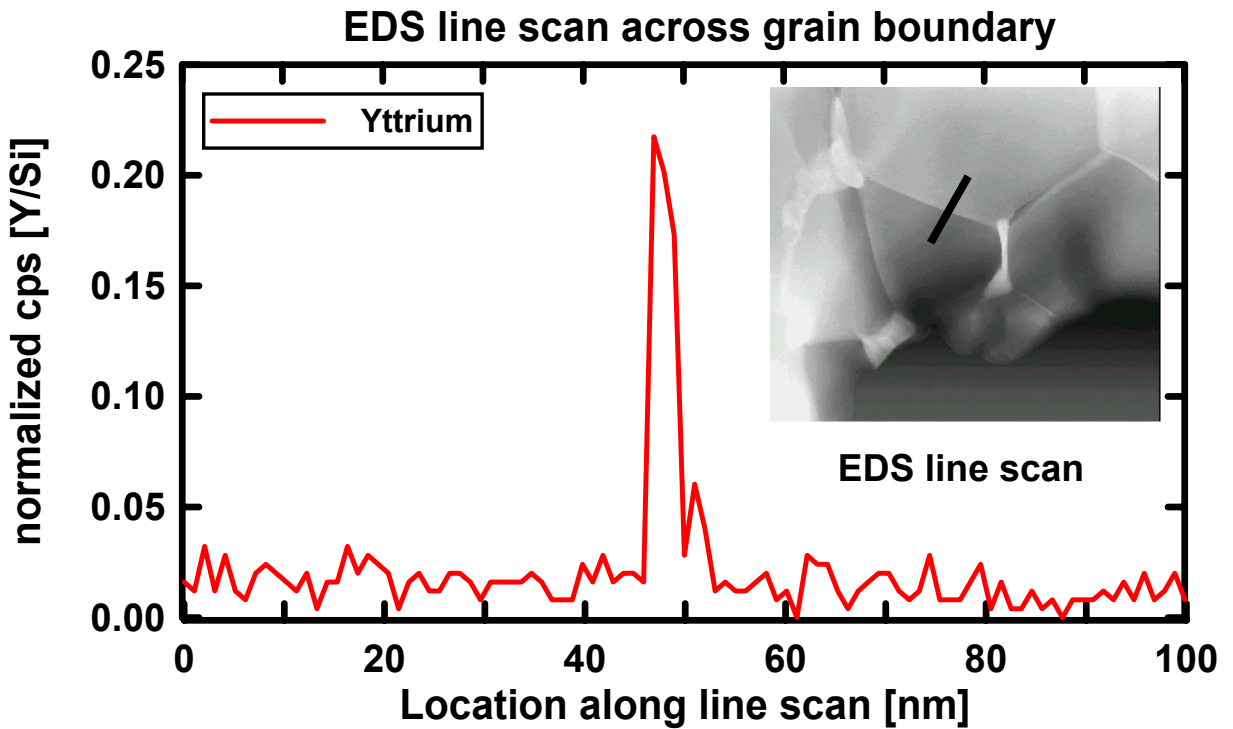


Figure 6

EDS line-scan taken across a thin grain boundary reveals the presence of yttrium ions segregated to the amorphous interface layer. It is expected that most of these Y-ions are not attached to the prism plane, instead they are located in the thin amorphous grain boundary layer.

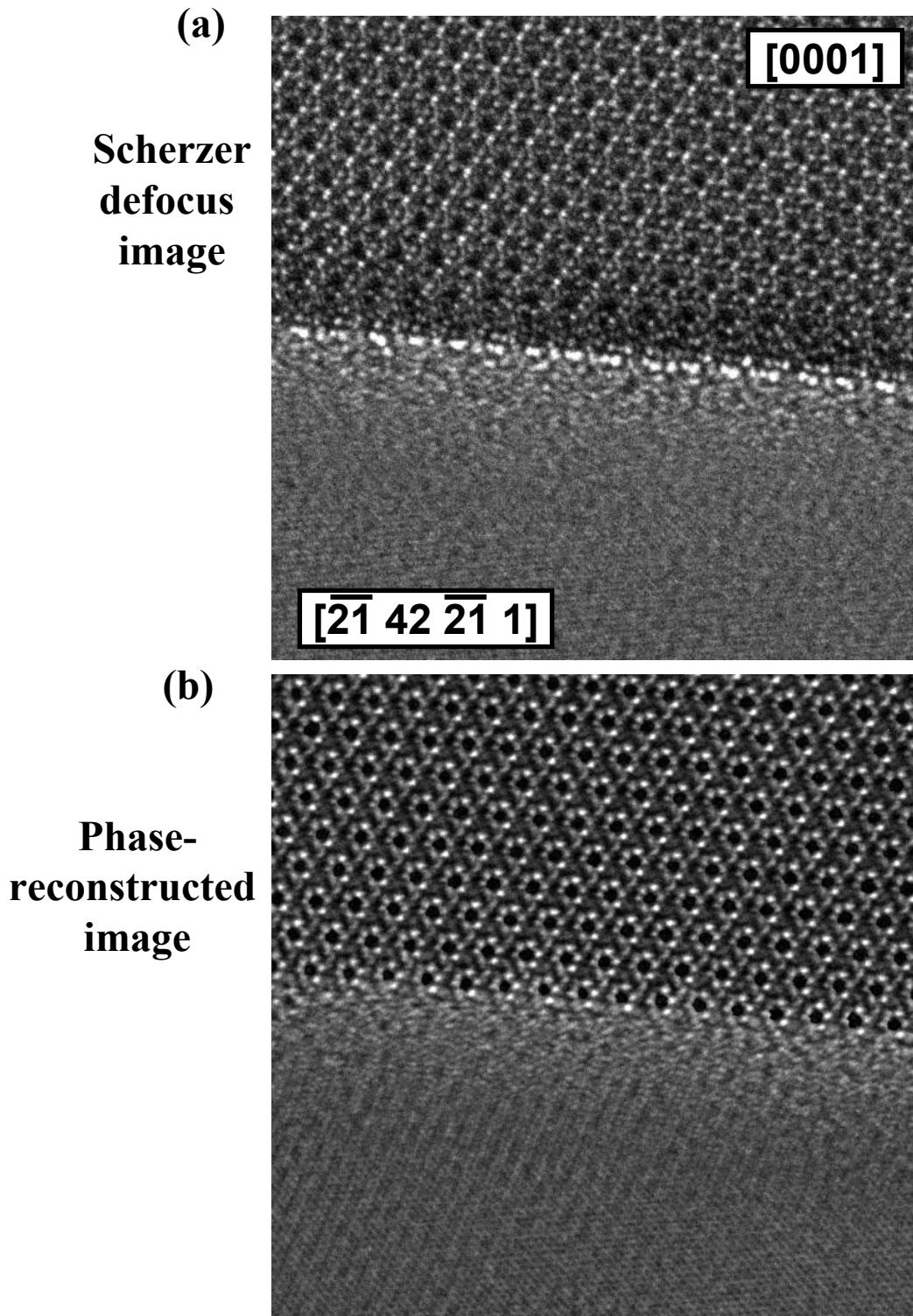


Figure 7

The Scherzer defocus (a) and the corresponding phase-reconstructed image (b) of a grain boundary are shown. The sample in this area is estimated to be thicker than the recommended specimen thickness for optimum phase reconstruction results. The Scherzer image displays bright spots that exhibit a very regular periodicity. These features disappear though in the phase reconstructed image.



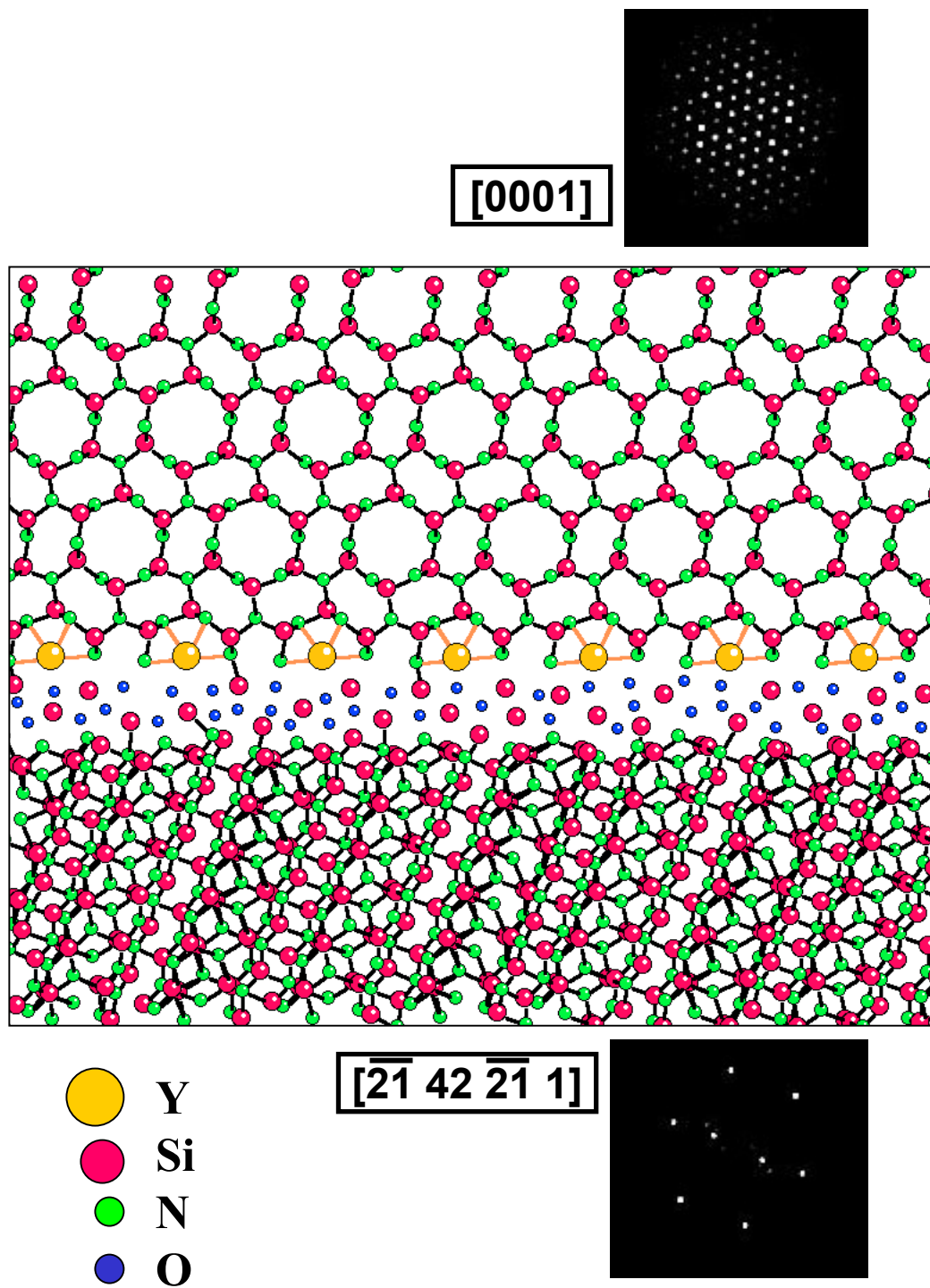
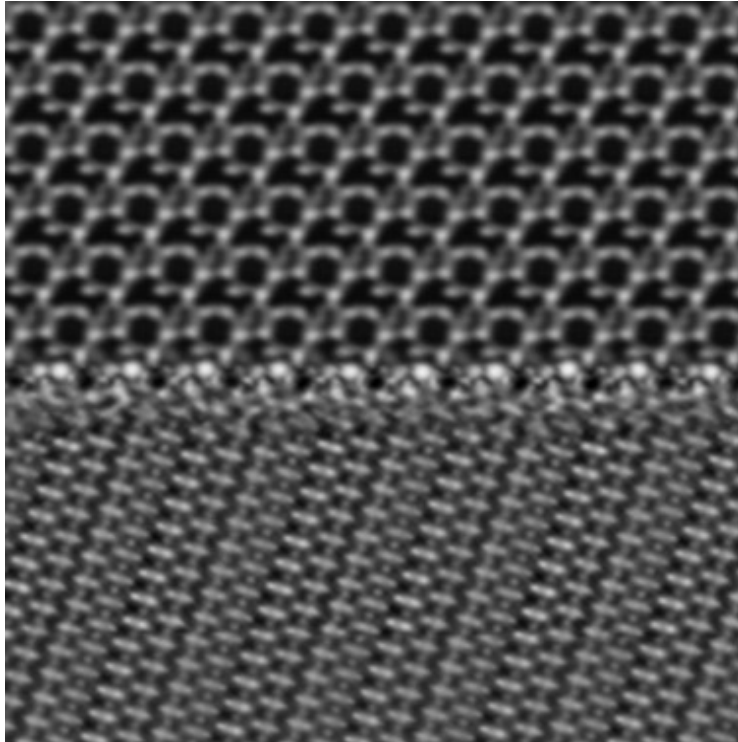


Figure 8  
 Grain boundary model used for computer simulation of the Scherzer and phase reconstruction images of Fig 7. Both crystals adjacent to the amorphous grain boundary layer are oriented exactly as in the experimental images.

**(a)**

**Scherzer  
defocus  
image of  
computer  
simulation**



**(b)**

**Phase-  
reconstructed  
image of  
computer  
simulation**

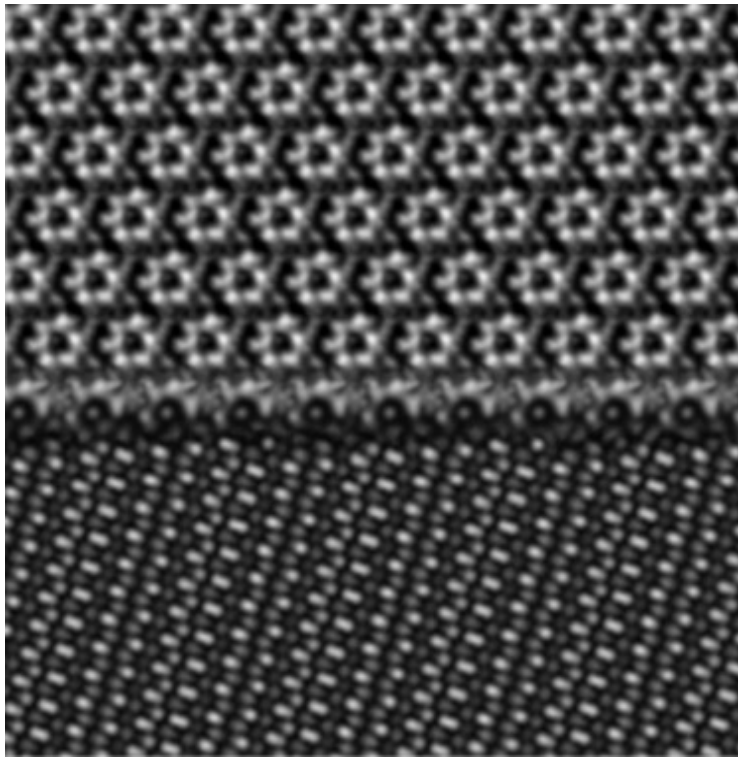


Figure 9

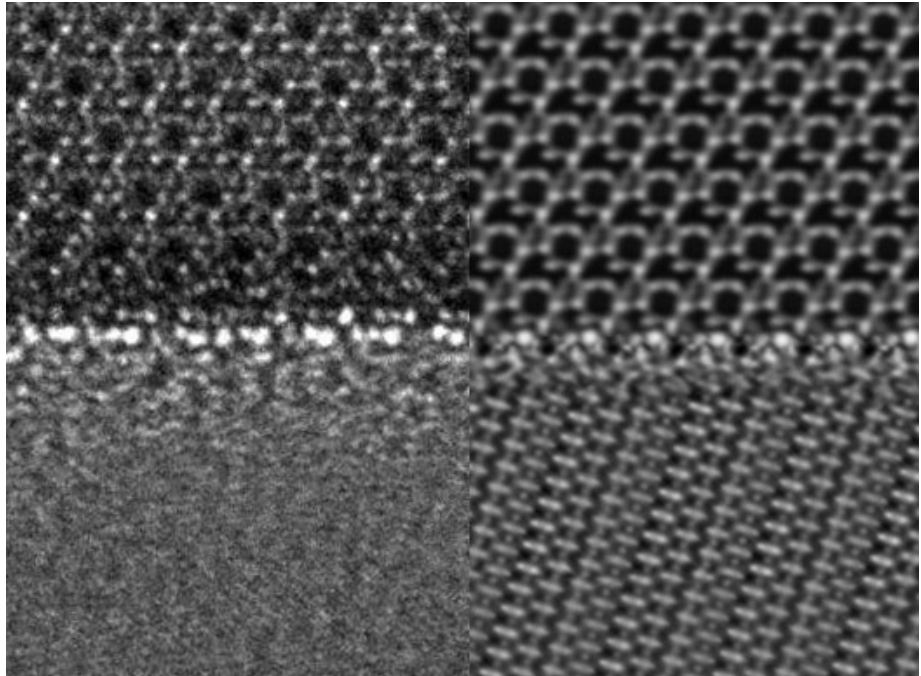
The simulated Scherzer defocus (a) and the corresponding simulated phase-reconstructed image (b) of the grain boundary from Fig. 7 are shown.

**Experiment**

**Simulation**

**(a)**

**Scherzer  
defocus  
images**



**(b)**

**Phase-  
reconstructed  
images**

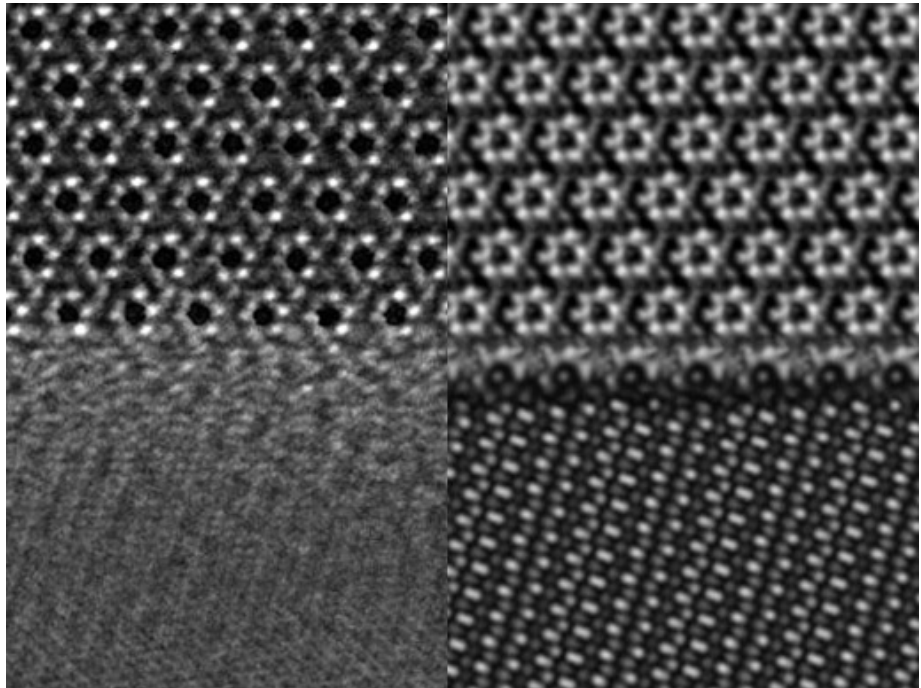


Figure 10

A direct comparison of the experimental and the computer-simulated images is presented. The images match well and similar features can be discerned.

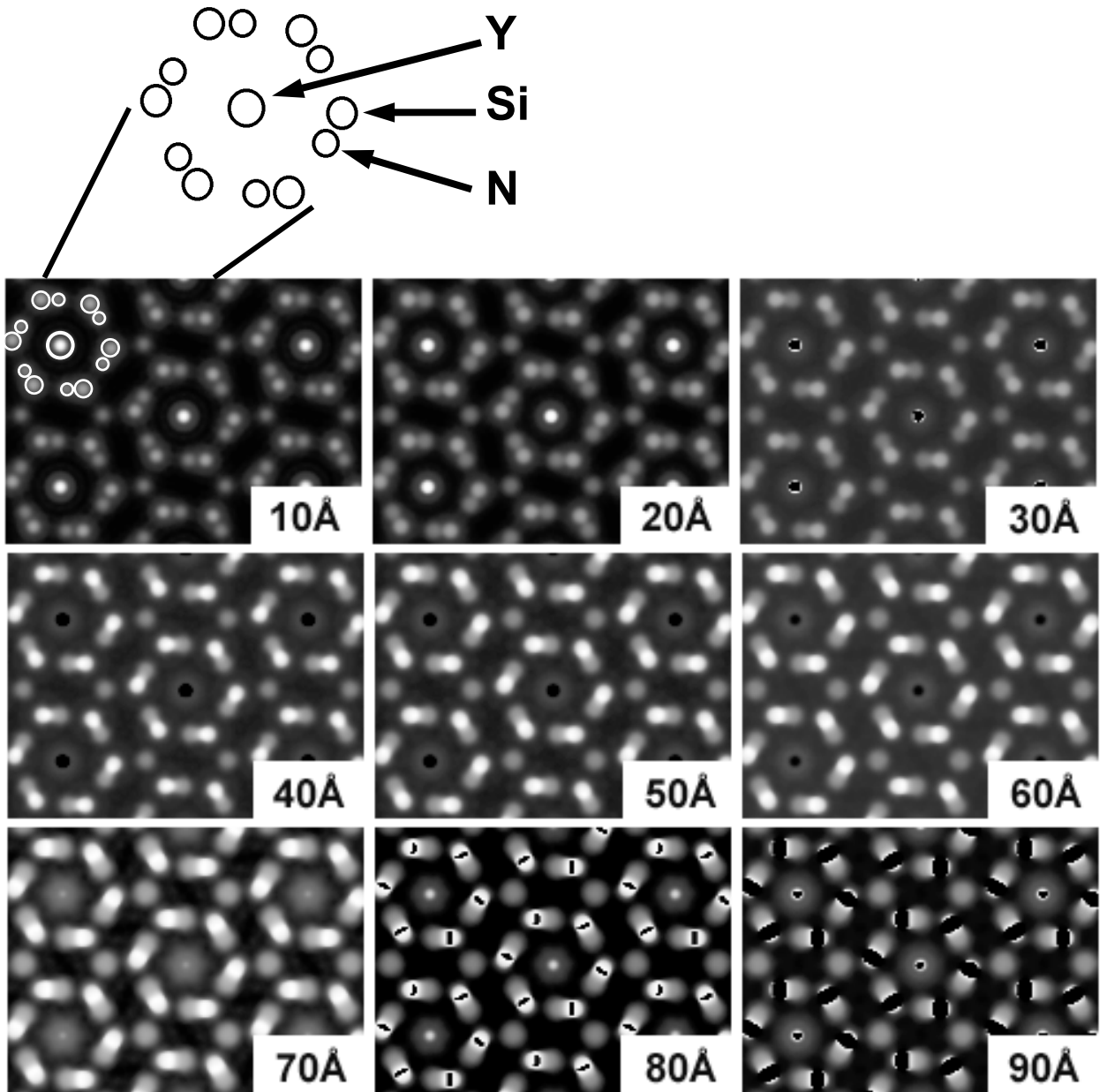


Figure 11

An array of computer-simulated images shows how the Y-signal oscillates when the sample thickness is varied. The brightness of the spot created by the Y-atom changes with thickness; it oscillates with the extinction distance  $\zeta$ .

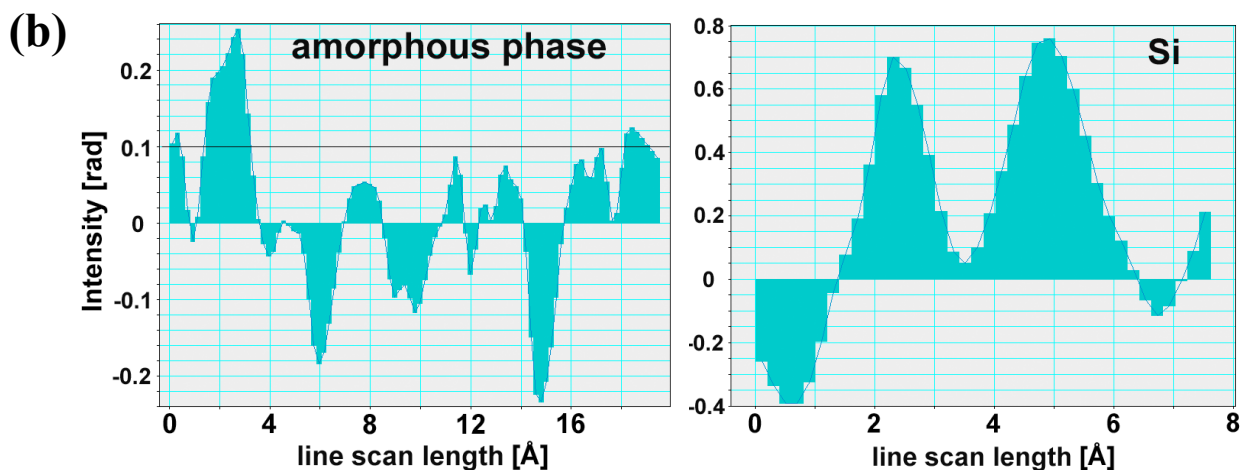
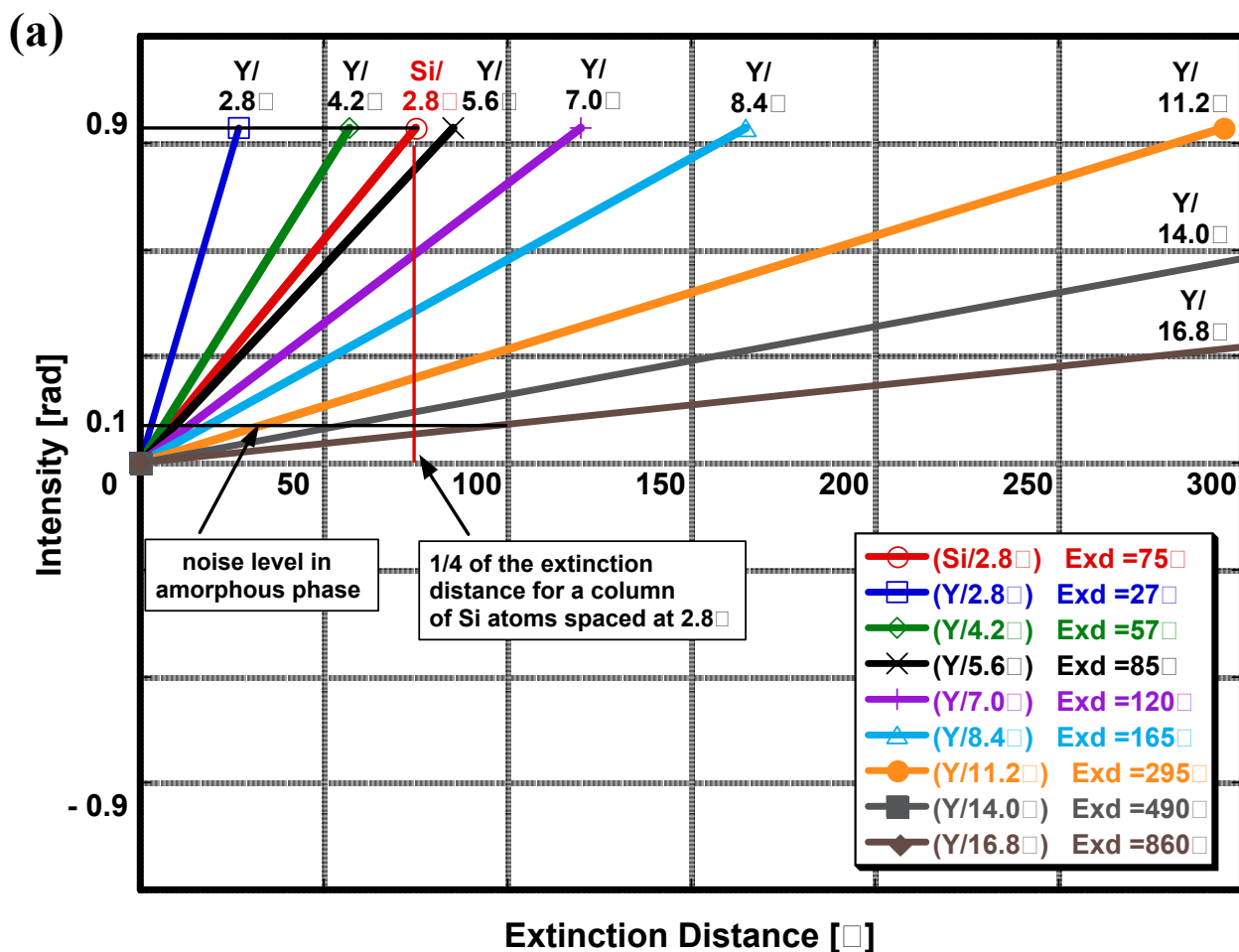


Figure 12

The graph shows how the extinction distance varies with line density and how Y compares to Si (a). For visibility criteria the noise level, (0.1rad) represented here by the amorphous phase and the maximum visible signal, (0.9rad) represented here by Si, are determined (b). A line density that results in a smaller signal than the noise level cannot be identified anymore in a TEM image.

**without Yttrium**

**with Yttrium**

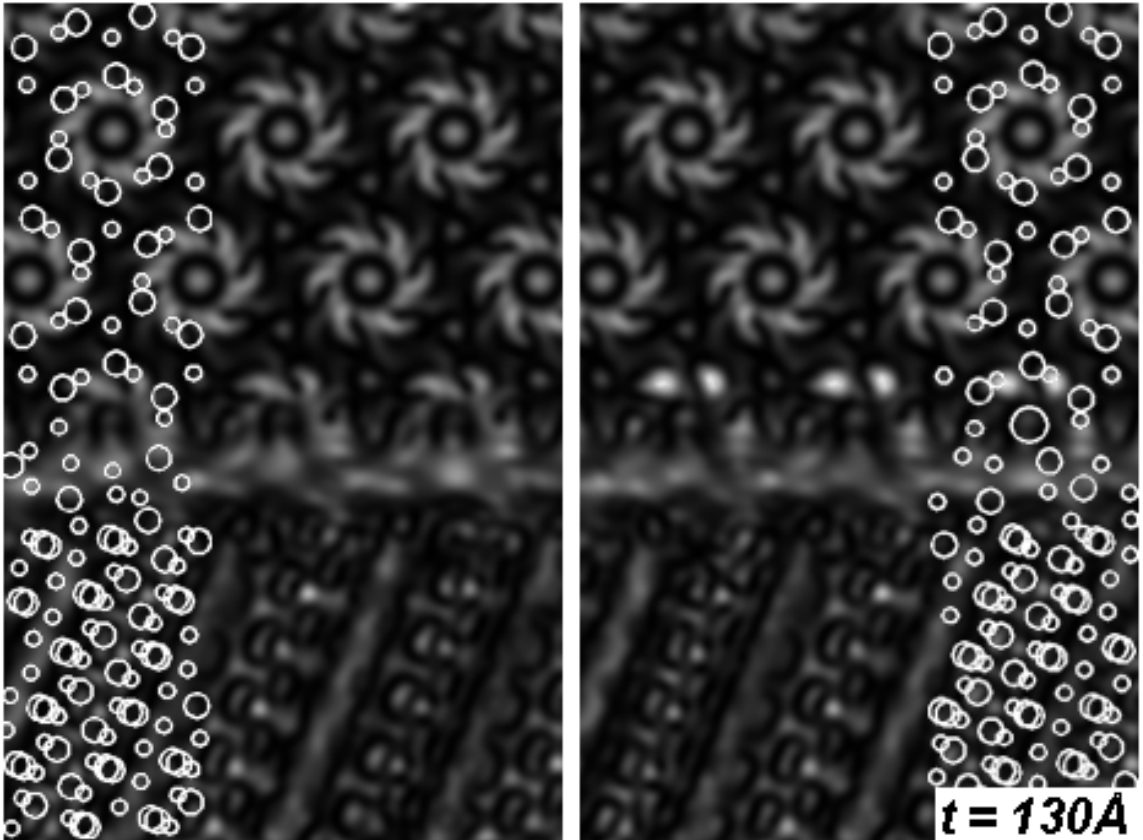


Figure 13

Simulated Scherzer defocus images of a grain boundary with and without yttrium at certain atomic positions (atom overlay) display different features. The array of bright spots in the image of the yttrium-containing grain boundary resembles the experimentally obtained Scherzer defocus image.